Energy 186 (2019) 115875

Contents lists available at ScienceDirect

Energy

journal homepage: www.elsevier.com/locate/energy

An irreversible Stirling cycle with temperature difference both in non-isothermal and isochoric processes

Dongdong Dai, Zhichun Liu, Rui Long, Fang Yuan, Wei Liu*

School of Energy and Power Engineering, Huazhong University of Science and Technology, Wuhan, 430074, PR China

ARTICLE INFO

Article history:
Received 24 February 2019
Received in revised form
6 July 2019
Accepted 2 August 2019
Available online xxx

Keywords:
Irreversible Stirling cycle
Non-isothermal process
Isochoric process
Temperature difference
Multi-objective optimization

ABSTRACT

In this paper, an irreversible thermodynamic cycle working between two constant temperature external reservoirs is proposed to model the practical Stirling engine by applying finite time thermodynamics (FTT). To analyze the regenerative processes, the regenerator is assumed to consist of numerous smaller heat reservoirs with individual temperature, and the irreversible heat transfer occurs between the working fluid and these smaller heat reservoirs. To analyze the expansive and compressive processes, polytropic processes are adopted to model the expansive and compressive processes, and corresponding polytropic exponents are obtained by thermodynamics for the first time. Based on the proposed thermodynamic model, the expression of thermal efficiency and output power are derived. In addition, the effects of thermodynamic parameters on power and efficiency are investigated to evaluate the performance of the proposed model. To optimize the proposed Stirling cycle model, an intelligent optimization algorithm named multi-objective particle swarm optimization based on crowding distance (MOPSOCD) is adopted to optimize the output power and thermal efficiency simultaneously.

1. Introduction

As a large amount of heat is released to the environment in heat-work conversion processes, Stirling engine has come to widely studied for its high heat-work conversion efficiency. Besides, the superiorities of Stirling engine as cleanness, reliability, and quietness attract more and more researchers and engineers' interests.

As an external heated engine with a regenerator, ideal Stirling engine consists of an external heating process, an external cooling process, and two regenerating processes. Stirling cycle, the ideal cycle model of Stirling engine, has the same efficiency with Carnot cycle, i.e. the highest heat-work conversion efficiency. However, in a practical Stirling engine, the working fluid does not follow the ideal Stirling cycle. To develop the guide of practical engines, Stirling engine's thermodynamic analysis has never been stopped since its inception [1–3].

Finite time thermodynamics (FTT) is a prevailing thermodynamics analysis method which was first proposed by Curzon and Ahlborn [4] to describe external irreversible Carnot cycle. The efficiency of Carnot cycle is the maximum efficiency with which thermal energy can be converted to mechanical energy. However, to achieve the ideal Carnot efficiency, the contact time must be infinite and results in zero power, which is impossible in practice. In FTT, being considered in finite time, thermodynamic processes are irreversible and the corresponding cycle efficiency is less than the ideal one. Following the effort made by Curzon and Ahlborn, much work has been carried out through FTT [5,6]. Blank et al. [7] applied FTT to Stirling engines to investigate the potential performance bounds. The model they proposed was based on a regenerator with perfect efficiency and external heat reservoirs with constant temperatures. They developed an endoreversible Stirling cycle model considering the thermal resistance in heat exchangers and optimized it to provide maximum power. Different from Blank, Ladas and Ibrahim [8] applying FTT to Stirling engine analysis by taking mass and energy balances with associated heat-transfer-rate equations into consideration, and found that based on engine speed and heat-transfer contact duration, there exists an optimum power output for a given engine design.

In the actual situation, as the regenerator is not perfect for regenerative heat loss, it is necessary to consider the imperfect regenerator when modeling the realistic Stirling engine. By defining a regenerative effectiveness, some scholars developed Stirling engine models with imperfect regenerators [9–17]. With the method of FTT, Wu et al. [13] developed a thermodynamic

* Corresponding author.
E-mail address: w_liu@hust.edu.cn (W. Liu).

https://doi.org/10.1016/j.energy.2019.115875
0360-5442/

model of imperfect Stirling engine and derived the relationship between the power and efficiency. Ding et al. [18] studied and optimized Stirling engine under a linear phenomenological law with irreversibility as heat resistance, heat leakage, regeneration loss and mechanical losses. Chen et al. [14] used FTT to investigate a solar Stirling system with the definition of regenerative effectiveness and obtained the thermal efficiency limit of the system. They also used the same method to develop thermodynamic models of Stirling heat pump [19] and refrigerator [20,21]. Considering the irreversible regenerative loss, Dai et al. [22] presented a detailed analysis of the regenerative processes instead of defining a regenerative effectiveness and obtained a more detailed Stirling engine model based on FTT. In addition, the thermal efficiency could be raised by the way of heat transfer enhancement in the heater, cooler and regenerator of Stirling engine [23,24].

In these cycle models, to ensure the isothermal assumptions in expansion and compression processes, the regenerative heat loss caused by temperature difference between the working fluid and regenerator, need to be additional supplied by heat reservoirs. However, in practice, there is no external heating process to supply regenerative heat loss and neither the expansion nor compression process is isothermal. Based on polytropic processes assumptions, Erbay et al. [25] developed a Stirling engine model with constant temperature heat reservoirs. They evaluated the model with several specific exponents of polytropic processes. The values of polytropic exponents in heating and cooling processes still need to be determined by thermodynamics.

As an effective and efficient optimization method, artificial-intelligence-based algorithms have been widely applied in physical and engineering optimization [26–30]. Among these algorithms, the genetic algorithm is a most general used algorithm in Stirling engine designs. With isothermal assumptions in expansion and compression process, Ahmadi et al. [31–33] took multi-objective optimization of Stirling engines using genetic algorithm. Duan et al. [34] applied the particle swarm optimization, an intelligent optimization algorithm with an advantage in searching speed, to Stirling engine optimization, result of which demonstrated a superiority compared with that of single-optimization method. Luo et al. [35] developed a multi-objective method consisting of three different kinds of algorithms to the optimization of GPU3 Stirling engine.

In previous studies on Stirling engine cycles, the expansion and compression processes are mainly based on ideal isothermal assumptions, and the imperfect regeneration is considered simply by defining a regenerative effectiveness. However, the isothermal requirement for expansion and compression processes is hard to fulfill due to the temperature difference between the working fluid and external heat reservoirs with constant temperature. The expansion and compression processes of a practical Stirling engine are closer to polytropic processes rather than isothermal processes. In addition, due to the temperature difference between the working fluid and porous materials in the regenerator, the irreversibility of heat transfer in regeneration should be considered. Thus, in this paper, a practical Stirling engine cycle model considering irreversible heat transfer both in the regeneration and polytropic processes is established with FTT. The expressions of thermal efficiency and output power are derived, and the effects of thermodynamic parameters on the cycle performance are investigated. To optimize the proposed model, a multi-objective optimization algorithm named MOPSOCD is adopted to optimize the thermal efficiency and output power simultaneously.

1.1. Analysis with finite time thermodynamics

The temperature-entropy diagram of Stirling engine with two constant-temperature external heat sources is depicted in Fig. 1. Previous FTT Stirling engine models considered the irreversibility caused by temperature difference in expansive and compressive processes. As a result, the compression stroke releasing heat to an external heat sink and expansion stroke absorbing heat from an external source are modeled as isothermal processes 1–2 and 3–4, respectively. The working fluid transfer heat from and to the regenerator are modeled as isochoric processes 2–3 and 4–1, respectively. In real Stirling engines, the efficiency of regenerator cannot reach 100%, which means the heat absorbed from and release to the regenerator cannot be as much as expected. Due to the imperfect regeneration, the outlet temperatures of working fluid during isochoric heating and cooling processes are $T_{3'}$ and $T_{1'}$, rather than T_3 and T_1. Due to the existence of thermal resistance, there is temperature difference between the working fluid and external heat reservoirs in finite time. As a result, the practical Stirling engine cycle is modeled as consists of two isochoric processes and two non-isothermal processes.

1.2. Regeneration

As a crucial component of Stirling engine cycle, the regeneration consists of a regenerative heating process to absorb heat from the regenerator and a regenerative cooling process to reject heat to the regenerator. An ideal regeneration is a quasistatic process, which means it needs to proceed with infinite time. In practice, however, the Stirling engine generally works with a high frequency and as a consequence the corresponding duration is short. As a result, the working fluid is disabled to get to the anticipated temperature when accomplishing the regeneration and the regenerator invariably follows an unevenly temperature distribution. Therefore, as depicted in Fig. 2, the regenerator is supposed to consist of numerous smaller heat reservoirs with individual temperatures. Heat transfer occurs when the working fluid contacts these smaller heat reservoirs sequentially during regenerative processes.

The working fluid of Stirling engine is usually a kind of gas like air, helium, or hydrogen. As the heat capacity of the working fluid is much smaller than that of the regenerator, we assume the temperature distribution of the sub-regenerator stays the same when the working fluid flows through the regenerator. Temperatures of *n*

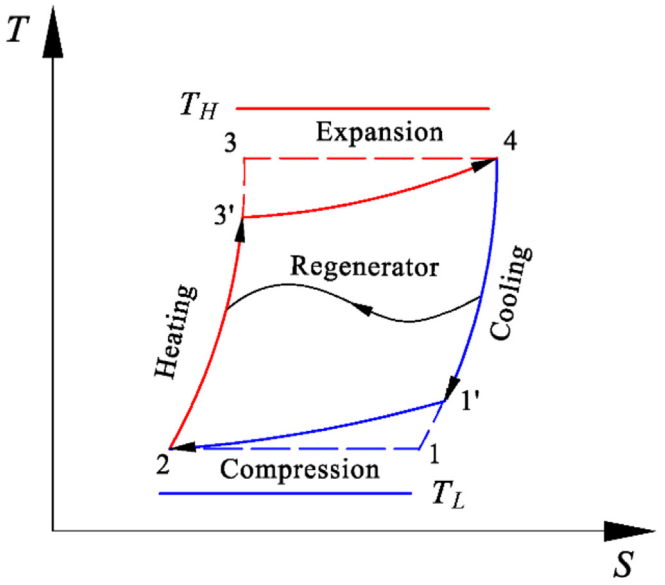

Fig. 1. The temperature-entropy diagram of the Stirling engine.

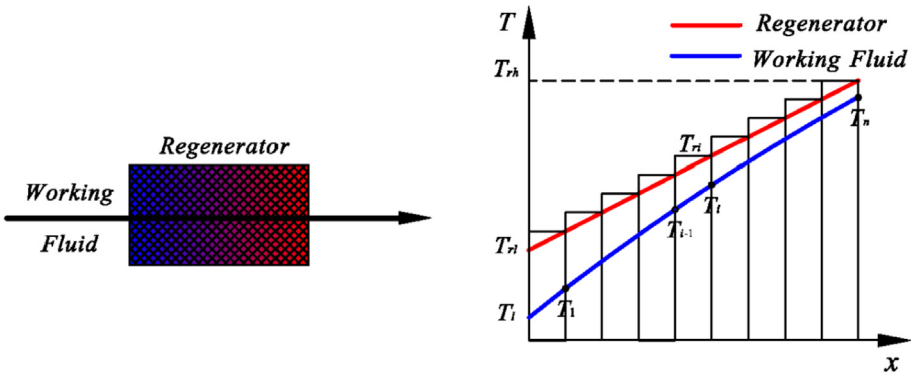

Fig. 2. Schematic diagram of temperature difference in regenerative heating process.

sub-regenerators are assumed to have individual temperatures varying from $T_l + \triangle T$ to $T_h - \triangle T$, and the constant temperature difference between adjacent sub-regenerators is $\triangle T$. Consequently, the constant temperature difference $\triangle T$ is given by

$$\Delta T = \frac{T_h - T_l}{n+1}. \tag{1}$$

Then the temperature of the ith sub-regenerator has the following expression as

$$T_{r,i} = T_l + \frac{T_h - T_l}{n+1} i, \quad i = 1, 2, \ldots, n. \tag{2}$$

Denote the entire duration of the regenerative heating process by t_r, and the working fluid flows through each sub-regenerator with the average time as

$$\Delta t = \frac{t_r}{n}. \tag{3}$$

The temperature of the working fluid leaving out of the compression chamber, and the ith sub-regenerator are T_l and $T_{r,i}$, respectively. We can know from the Newton's law of cooling that the rate of heat absorbs by the working fluid is proportional to the heat transfer coefficient and temperature difference between it and the ith sub-regenerator, i.e.,

$$\delta Q_i = h_r A_r \left(T_{r,i} - T_{f,i}\right) dt, \quad i = 1, 2, \ldots, n, \tag{4}$$

where h_r and A_r are the convective heat transfer coefficient and the contact area, respectively. For convenience, we denote the product of h_r and A_r as α_r. As there is no volume variation during regeneration, all the heat transferred to the working fluid is used to promote its internal energy, i.e.,

$$\delta Q_i = m c_v dT_{f,i}, \quad i = 1, 2, \ldots, n. \tag{5}$$

By substituting Eq. (4) into Eq. (5), we have the relationship between $T_{r,i}$ and $T_{f,i}$ as

$$dt = \frac{\Sigma dT_{f,i}}{\left(T_{r,i} - T_{f,i}\right)}, \quad i = 1, 2, \ldots, n, \tag{6}$$

where $\Sigma = m c_w / \alpha_r$. According to the equations above we can get the relationship between $T_{f,i}$ and $T_{f,i\text{-}1}$ as

$$\frac{T_{r,i} - T_{f,i-1}}{T_{r,i} - T_{f,i}} = e^{\frac{t_r}{n\Sigma}}, \quad i = 1, 2, \ldots, n. \tag{7}$$

By substituting Eq. (2) into Eq. (7), we can obtain the expression of $T_{f,i}$ by iteration as

$$T_{f,i} = T_l + \frac{T_h - T_l}{n+1}\left(i - \frac{e^{-\frac{t_r}{n\Sigma} i} - 1}{1 - e^{\frac{t_r}{n\Sigma}}}\right), \quad i = 1, 2, \ldots, n. \tag{8}$$

When $i = n$, $T_{f,i}$ can be written as $T_{f,n}$, representing the temperature that working fluid reaches after transferring heat with n sub-regenerators. The temperature of working fluid reaches its maximal value after the entire regenerative heating process, which can be stated as

$$T_{f,n} = T_l + \frac{T_h - T_l}{n+1}\left(n + \frac{1 - e^{-\frac{t_r}{\Sigma}}}{1 - e^{\frac{t_r}{n\Sigma}}}\right). \tag{9}$$

The regenerative effectiveness, defined as the ratio of heat transfer in real to that in ideal during regenerative processes, can be determined by the following expression,

$$e_r = \frac{Q_{real}}{Q_{ideal}} = \frac{T_{f,n} - T_l}{T_h - T_l} = \frac{n - \frac{1 - e^{\frac{t_r}{\Sigma}}}{e^{\frac{t_r}{\Sigma}} - e^{\frac{t_r}{\Sigma}\left(\frac{1}{n}+1\right)}}}{n+1}. \tag{10}$$

In a similar way, we can obtain the same expression for regenerative cooling effectiveness in the same duration t_r.

When $n \to \infty$, which means there are infinite sub-regenerators, the regenerative effectiveness can be simplified as

$$e_r = 1 - \frac{\Sigma}{t_r}\left(1 - e^{-\frac{t_r}{\Sigma}}\right). \tag{11}$$

In practice, due to the finite values of Σ and t_r, e_r is a number less than 1, indicating the imperfection of regeneration. According to the definition of regenerative efficiency, the outlet temperatures of the working fluid for regenerative cooling and heating processes can be stated as

$$T_{1'} = T_1 + \frac{\Sigma}{t_r}\left(1 - e^{-\frac{t_r}{\Sigma}}\right)(T_4 - T_1), \tag{12}$$

and

$$T_{3'} = T_3 - \frac{\Sigma}{t_r}\left(1 - e^{-\frac{t_r}{\Sigma}}\right)(T_3 - T_2). \tag{13}$$

1.3. Expansion process

In the expansion process, the working fluid absorbs heat from the external heat source with a constant temperature T_h, and in the meantime, the expansive work is produced. Due to the imperfect regeneration, the working fluid's initial temperature in the expansion process is $T_{3'}$, which is unequal to its final temperature in the expansion stroke T_4. That means the expansion process of a Stirling engine is a non-isothermal process, which conflicts with the fact that the expansion and compression processes of the ideal Stirling cycle are isothermal processes. To investigate the thermodynamic process in the expansion space, we will take the polytropic process into consideration.

Denote the index of the polytropic expansive process by n_1, then the relationship of pressure and volume can be described as

$$pV^{n_1} = c_1. \tag{14}$$

The ideal gas equation of state of the working fluid is given by

$$pV = mR_gT. \tag{15}$$

Then the relationship of volume and temperature of the working fluid during the expansion process can be stated as

$$TV^{n_1-1} = \frac{c_1}{mR_g}. \tag{16}$$

At the initial and final states of working fluid in the expansion process, i.e., states 3′ and 4, the relationships can be obtained as

$$\begin{cases} T_{3'}V_{3'}^{n_1-1} = \dfrac{c_1}{mR_g} \\ T_4V_4^{n_1-1} = \dfrac{c_1}{mR_g} \end{cases}. \tag{17}$$

Then the polytropic index n_1 and constant c_1 can be derived as

$$n_1 = \frac{\ln(T_{3'}/T_4)}{\ln(V_4/V_{3'})} + 1, \tag{18}$$

and

$$c_1 = mR_gT_4V_4^{\frac{\ln(T_{3'}/T_4)}{\ln(V_4/V_{3'})}}. \tag{19}$$

The regenerative effectiveness in Eq. (10) can be written in terms of $T_{3'}/T_4$ as follows:

$$e_r = \frac{Q_{real}}{Q_{ideal}} = \frac{c_vm(T_{3'} - T_2)}{c_vm(T_4 - T_2)} = \frac{\frac{T_{3'}}{T_4} - \gamma}{1 - \gamma}, \tag{20}$$

where $\gamma = T_2/T_4$. By substituting Eq. (20) into Eq. (18) – (19), the polytropic index n_1 and constant c_1 can be obtained as

$$n_1 = \frac{\ln(e_r + (1 - e_r)\gamma)}{\ln\lambda} + 1, \tag{21}$$

and

$$c_1 = mR_gT_4V_4^{\frac{\ln(e_r + (1-e_r)\gamma)}{\ln\lambda}}, \tag{22}$$

where $\lambda = V_1/V_2 = V_4/V_3$.

The rate of heat transfer into the working fluid is proportional to the temperature difference between the working fluid and heat source according to the heat transfer theory. Thus, we state the heat transfer during the expansion process as

$$\delta Q_h = \alpha_h(T_h - T)dt, \tag{23}$$

where Q_h denotes the amount of heat transfers in the expansion process, α_h denotes the thermal conductance between the working fluid and heat source.

As the first law of thermodynamics describes, the heat absorbed by the working fluid is used to increase its internal energy and produce work

$$\delta Q_h = mc_vdT + pdV. \tag{24}$$

Combining Eqs. (23) and (24), the relationship of time and volume of working fluid during the expansion process can be obtained as

$$dt = \frac{c_1\left(\frac{c_v}{R_g}(1 - n_1) + 1\right)}{\alpha_h\left(T_HV^{n_1} - \frac{c_1V}{mR_g}\right)}dV. \tag{25}$$

Integrating the above equation and considering the initial and final state of the working fluid in the expansion process, the expansion duration can be expressed as

$$t_h = \frac{m(c_v(1 - n_1) + R_g)}{\alpha_h(n_1 - 1)}\ln\frac{mR_gT_H - c_1V_4^{1-n_1}}{mR_gT_H - c_1V_3^{1-n_1}}. \tag{26}$$

The expansion work can be calculated as

$$W_h = \int_{V_{3'}}^{V_4} pdV = \frac{1 - \lambda^{n_1-1}}{1 - n_1}mR_gT_h. \tag{27}$$

In the expansion process, the absorbed heat is used to produce work and promote the internal energy of the working fluid, which can be expressed as

$$Q_h = W_h + \Delta U = \frac{1 - \lambda^{n_1-1}}{1 - n_1}mR_gT_h + mc_v(1 - e_r)(T_h - T_l). \tag{28}$$

1.4. Compression process

In the compression process, the working fluid rejects heat to a heat sink with a constant temperature. For the same reason in the regenerative rejecting heat process, the initial temperature of working fluid in compression space is $T_{1'}$ rather than T_1, while the final temperature of working fluid in compression process is T_2. That means the compression process of the Stirling engine is also a non-isothermal process, which conflicts with the assumption of the ideal Stirling cycle that the compression process is isothermal. To investigate the process in compression space, we will take the polytropic process into consideration as well.

Denote the index of the polytropic compressive process by n_2, then the relationship of pressure and volume can be described as

$$pV^{n_2} = c_2. \tag{29}$$

According to the ideal gas equation of state, the relationship of volume and temperature can be derived as

$$TV^{n_2-1} = \frac{c_2}{mR_g}. \tag{30}$$

At the initial and final states of working fluid in the expansion process, i.e., states 1′ and 2, the relationships can be obtained as

$$\begin{cases} T_{1'}V_{1'}^{n_2-1} = \dfrac{c_2}{mR_g} \\ T_2V_2^{n_2-1} = \dfrac{c_2}{mR_g} \end{cases}. \tag{31}$$

Then the polytropic index n_2 and constant c_2 can be derived as

$$n_2 = \frac{\ln(T_2/T_{1'})}{\ln(V_{1'}/V_2)} + 1, \tag{32}$$

and

$$c_2 = mR_gT_2V_2^{\frac{\ln(T_2/T_{1'})}{\ln(V_{1'}/V_2)}}. \tag{33}$$

The regenerative effectiveness in Eq.(10) can be written in terms of $T_{1'}/T_4$ as follows:

$$e_r = \frac{Q_{real}}{Q_{ideal}} = \frac{c_vm(T_4 - T_{1'})}{c_vm(T_4 - T_2)} = \frac{1 - \frac{T_{1'}}{T_4}}{1 - \gamma}, \tag{34}$$

where $\gamma = T_2/T_4$. By substituting Eq. (34) into Eqs. (32),(33), the polytropic index n_2 and constant c_2 can be obtained as

$$n_2 = \frac{\ln\left(\frac{\gamma}{(1-e_r)+e_r\gamma}\right)}{\ln\lambda} + 1, \tag{35}$$

and

$$c_2 = mR_gT_2V_2^{\frac{\ln\left(\frac{\gamma}{(1-e_r)+e_r\gamma}\right)}{\ln\lambda}}, \tag{36}$$

The compression process is also a non-isothermal process because the initial temperature of the working fluid in compression space is not low enough to T_1 but $T_{1'}$ after the imperfect regenerative process 4–1′. Denote the temperature of the heat sink by T_l and the heat absorbed by the heat sink in compression Q_l is determined by the following expression

$$\delta Q_l = \alpha_l(T - T_l)dt, \tag{37}$$

where Q_l denotes the amount of heat transfers in the compression process, α_l denotes the thermal conductance between the working fluid and external heat sink.

As the first law of thermodynamics describes, the heat released to the heat sink has the same amount to the change in internal energy of working fluid plus the work done by the working fluid, which can be written as follows

$$-\delta Q_l = mc_vdT + pdV. \tag{38}$$

Combining Eqs. (37) and (38), the relationship of time and volume of working fluid during the compression process can be obtained as

$$dt = \frac{c_2\left(\frac{c_v}{R_g}(1-n_2)+1\right)}{\alpha_l\left(T_lV^{n_2} - \frac{c_2V}{mR_g}\right)}dV. \tag{39}$$

Integrating the above equation and considering the initial and final states of the working fluid in the compression process, the compression duration can be expressed as

$$t_l = \frac{m(c_v(1-n_2)+R_g)}{\alpha_l(n_2-1)}\ln\frac{mR_gT_L - c_2V_2^{1-n_2}}{mR_gT_L - c_2V_1^{1-n_2}}. \tag{40}$$

The compression work can be calculated as

$$W_l = -\int_{V_{1'}}^{V_2} pdV = \frac{\lambda^{1-n_2}-1}{1-n_2}mR_gT_l. \tag{41}$$

1.5. Performance of the model

As there is no volume change during regenerative processes, the work is only produced during the expansion and compression processes, which can be expressed as

$$W = W_h - W_l = \left(\frac{1-\lambda^{n_1-1}}{1-n_1}T_h - \frac{\lambda^{1-n_2}-1}{1-n_2}T_l\right)mR_g. \tag{42}$$

Then the thermal efficiency of the cycle can be developed as

$$\eta = \frac{W}{Q_h} = \frac{\frac{1-\lambda^{n_1-1}}{1-n_1} - \frac{\lambda^{1-n_2}-1}{1-n_2}\gamma}{\frac{1-\lambda^{n_1-1}}{1-n_1} + (1-e_r)(1-\gamma)\frac{c_v}{R_g}}. \tag{43}$$

The cyclic duration of Stirling engine can be calculated as

$$\tau = t_h + t_l + 2t_r. \tag{44}$$

The power output can be obtained by dividing the net cycle work by the cyclic time, which can be expressed as

$$P = \frac{W}{\tau} = \frac{\left(\frac{1-\lambda^{n_1-1}}{1-n_1}T_h - \frac{\lambda^{1-n_2}-1}{1-n_2}T_l\right)mR_g}{t_h + t_l + 2t_r}. \tag{45}$$

2. Sample calculations and discussion

In order to analyze the performance of this cycle model, we take helium as the working fluid for instance and design parameters of the Stirling engine are given as $m = 4$ g, $c_v = 3.21$ J/(g·K), $R_g = 2.08$ J/(g·K), $T_h = 1000$ K, $T_l = 300$ K, $\alpha_r = 20$ kJ/(K·s), $\alpha_h = 2$ kJ/(K·s), $\alpha_l = 2$ kJ/(K·s), $T_2 = 400$ K, $T_4 = 800$ K, $t_r = 0.005$ s. Computing with MATLAB and REFPROP developed by NIST (National Institute of Standard and Technology), the temperature-entropy and pressure-volume diagrams of working fluid in this model are plotted in Fig. 3.

As shown in Fig. 3, the ideal Stirling cycle is drawn in black and the processes of the model presented in this study are drawn in red. In an actual situation, an isochoric process is easy to proceed and we consider the regenerative processes are the same as the ideal cycle but the final status is different from that of the ideal cycle due to the regenerative loss. As a result, the regenerative processes are 4-1′ rather than 4-1 and 2–3′ rather than 2–3 as shown in Fig. 3. In the ideal cycle, the output power and thermal efficiency of Stirling

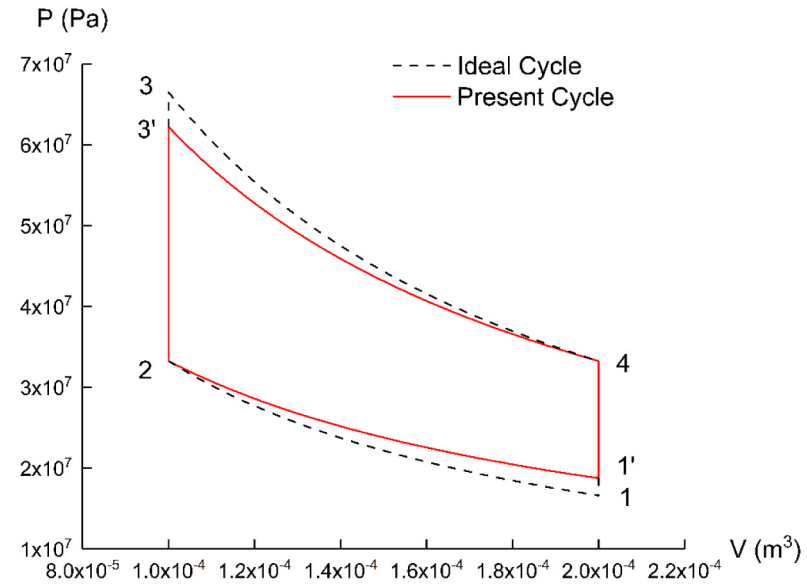

(a)

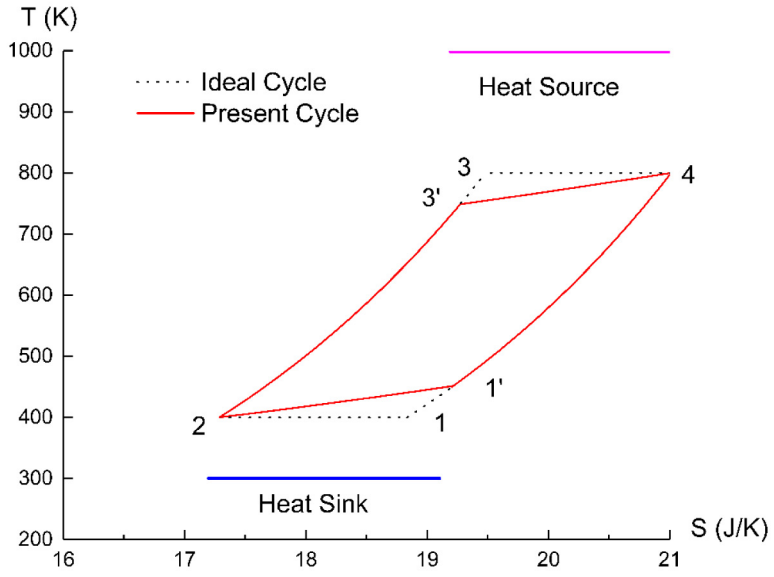

(b)

Fig. 3. The comparisons of Stirling cycle model in pressure-volume diagram (a); temperature-entropy diagram (b).

engine are 8.30 kW and 50%, respectively. For this Stirling engine model, according to Eqs. (43) and (45), the output power is 7.24 kW, and thermal efficiency is 39.25%, which are reduced by 1.06 kW and 10.75%, respectively.

2.1. Parametric study

A parametric study was conducted to observe the effects of the mass of working fluid m, thermal conductance in the expansion stroke α_h, thermal conductance in the expansion stroke α_l, regenerative duration t_r, and volume compression ratio λ on output power and thermal efficiency of Stirling engine. Helium is chosen as the working fluid in this Stirling engine model. Parameters m, α_h, α_l, t_r, and λ are varied as Table 1 shows to demonstrate the trends. For convenience, other parameters are set as the same as mentioned above. The results of the study are presented in Figs. 4–8.

It can be observed from Fig. 4 that when the mass of working fluid increases from 2.5 g to 7 g, the output power increases from 7.7 kW to 20.3 kW while the thermal efficiency decreases from 43.4% to 33.9%. When operating at a larger mass, the working fluid expanses and compresses at higher pressure and as such produces more cycle net work, which causes the output power increases.

Table 1
Ranges of studied parameters.

Parameter	Range	Unit
m	2.5–7	g
α_h	4–22	kW/K
α_l	4–22	kW/K
t_r	0.015–0.105	s
λ	2–6	–

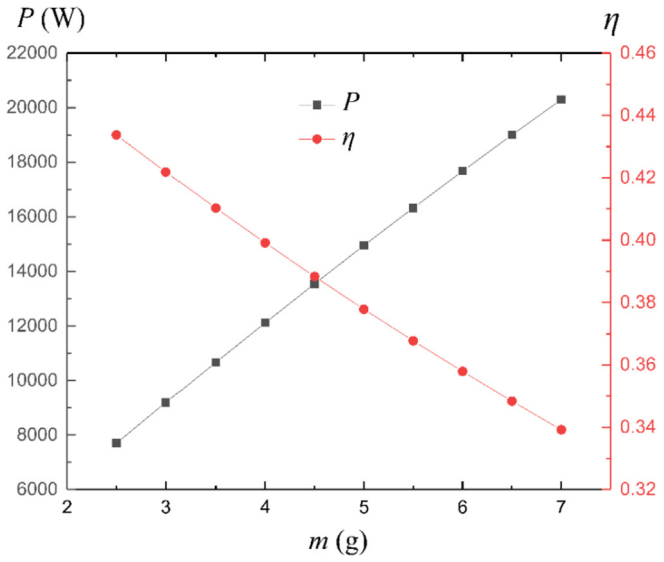

Fig. 4. Power and efficiency versus mass of working fluid.

With fixed specific heat capacity c_v and heat transfer parameter α_r, a larger mass of the working fluid leads to a lower regenerative effectiveness, and then bring down the thermal efficiency of the Stirling engine. As there is a conflict between output power and thermal efficiency in term of the mass of working fluid, a decision-

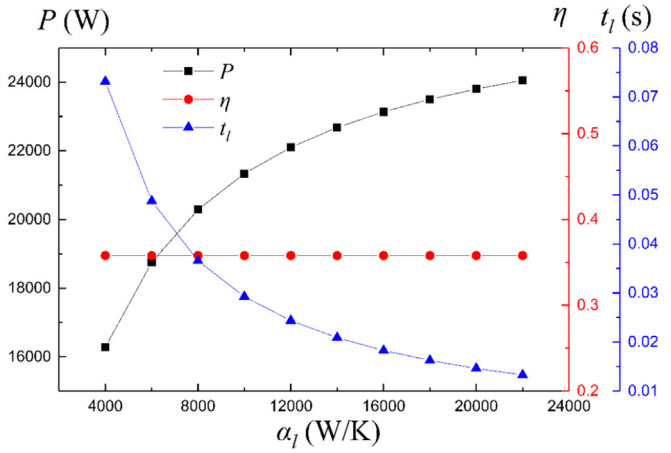

Fig. 6. Power, efficiency and heating time versus thermal conductance in the compression stroke.

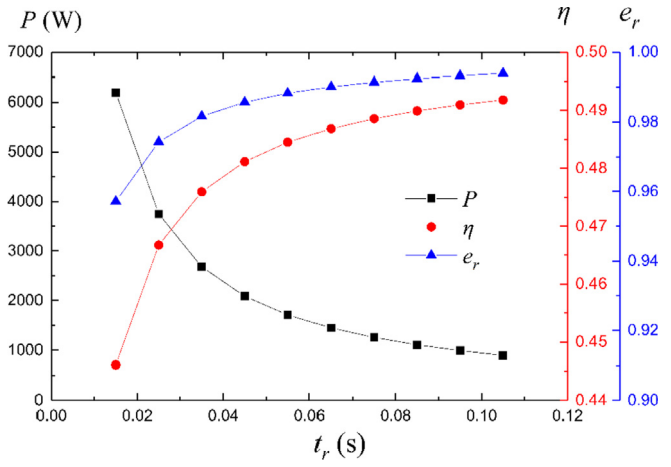

Fig. 7. Power, efficiency and regenerative effectiveness versus regenerative time.

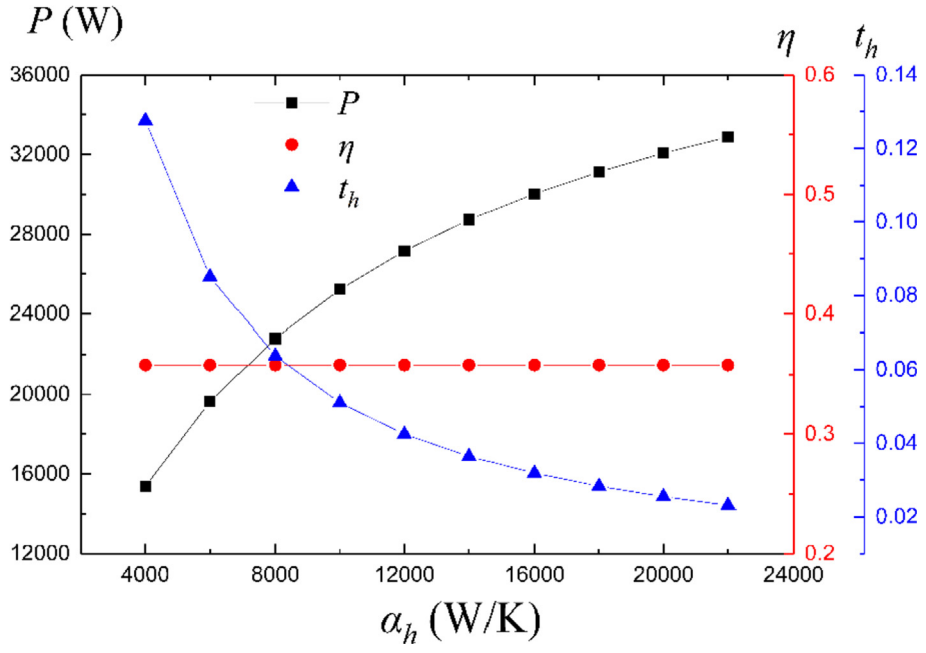

Fig. 5. Power, efficiency and heating time versus thermal conductance in expansion stroke.

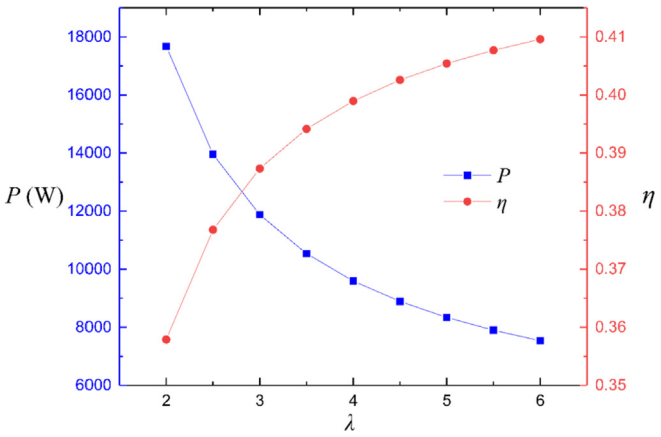

Fig. 8. Power and efficiency versus volume compression ratio.

making is necessary to make the Stirling engine perform well. In practice, the maximum pressure should be taken into consideration when increasing the mass of the working fluid.

As shown in Fig. 5, with the thermal conductance in the expansion stroke increases from 4000 W/K to 22000 W/K, the power output increases from 15.4 kW to 32.9 kW, the required heating time decreases from 0.128 s to 0.023 s while the thermal efficiency stays constant. A larger thermal conductance means in a greater ability to transfer heat, resulting in a shorter time to transfer a certain amount of heat. It can be observed from Eq. (34) that the thermal efficiency has no relationship with the thermal conductance in the expansion stroke. Therefore, a large heat conductance in the expansion stroke is necessary to improve the output power of the Stirling engine.

The effect of the thermal conductance in the compression stroke on output power, thermal efficiency, and required cooling time in the compression stroke are shown in Fig. 6. We can observe that when the thermal conductance in the compression stroke increases from 4000 W/K to 22000 W/K, the power output increases from 16.3 kW to 24.1 kW, the required heating time decreases from 0.07 s to 0.001 s while the thermal efficiency stays constant. For the same reason with that in the expansion stroke, a large thermal conductance in the compression stroke is beneficial to the performance of Stirling engine.

The effects of the regenerative time on output power, thermal efficiency, and regenerative effectiveness are represented in Fig. 7. With the regenerative time increases, the thermal efficiency and effectiveness increase with decreasing accelerated speeds while the output power decreases with a decreasing accelerated speed. When the working fluid flows through the regenerator, the heat transfers more sufficiently with a longer regenerative time. Therefore, the regenerative effectiveness and thermal efficiency increase as more heat is utilized. Nevertheless, for the output power, when the regenerative time increases, the effect of cycle duration outweighs that of the cycle work according to the results obtained in Fig. 7.

Fig. 8 shows the effects of volume compression ratio on power and efficiency. Non-linear trends are observed from Fig. 8: with the volume compression ratio increases, the thermal efficiency increases rapidly at first, and then slightly; while the output power decreases rapidly at first, and then slightly. Therefore, a high volume compression ratio leads to high output power but low thermal efficiency. As there is a conflict between output power and thermal efficiency in term of the compression ratio, a decision-making is necessary to make the Stirling engine perform well.

2.2. Multi-objective optimization

With respect to the optimization of a Stirling engine, objective functions like output power and thermal efficiency always conflict with each other. For example, in Fig. 8, with the volume compression ratio increases, the thermal efficiency increases while the output power decreases. In this section, an intelligence optimization algorithm, multi-objective optimization particle swarm optimization based on crowding distance (MOPSOCD) [36], is adopted to optimize the proposed Stirling cycle model.

As a population-based stochastic algorithm, the particle swarm optimization algorithm is heuristic inspired by the social behavior of bird flocking. In the beginning, some numerical vectors, which are conceptualized as particle swarm, are randomly initialized in the objective space. With the algorithm proceeds, the particle swarm moves towards the optimal regions in the objective space, and dynamically adjust the speed based on the integrated analysis of the individual and collective flight experience over generations. At each step, the particle updates its position by adding the velocity to its previous position. So the position of the ith particle in the tth step can be calculated by

$$\mathbf{x}_i^{(t)} = \mathbf{x}_i^{(t-1)} + \mathbf{v}_i^{(t)} \tag{46}$$

The velocity of each particle is updated by the following equation

$$\mathbf{v}_i^{(t+1)} = \alpha \mathbf{v}_i^{(t)} + \beta_1 \left(\mathbf{p}_i - \mathbf{x}_i^{(t)} \right) + \beta_2 \left(\mathbf{p}_g - \mathbf{x}_i^{(t)} \right) \tag{47}$$

where $\mathbf{p}$ is the best position found so far by the ith particle, g is the index of the ith particle's best neighbor, α is an inertia weight, β_1 and β_2, generated randomly in the range (0, 1), are called acceleration constants.

With the program process, if the current position is better than $\mathbf{p}$, $\mathbf{p}$ will be replaced by the current position. As a result, the particles swarm cluster together in optimal regions of the objective space, i.e., the Pareto frontier. PSO is an intelligent optimization algorithm with a strong convergence ability but it is easy to lose the diversity of solutions and trapped in a local optimum.

To maintaining the diversity of the solutions and avoid being trapped in local optimum, the crowding distance is adopted in the MOPSOCD algorithm to deal with multi-objective optimizations. As shown in Fig. 9, with respect to particle i, the mean distance of its

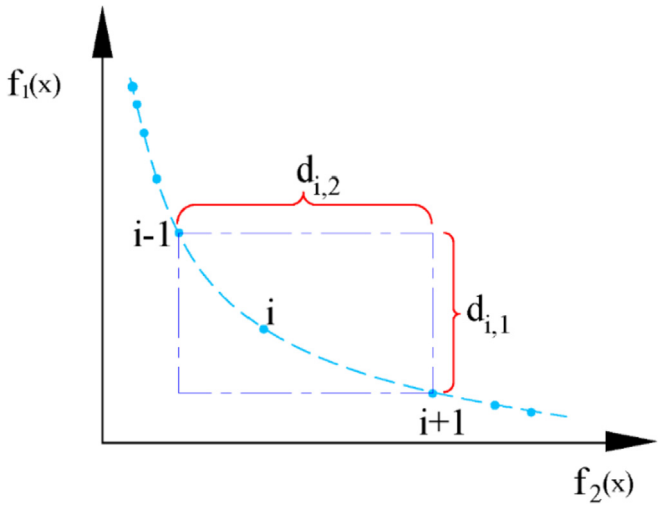

Fig. 9. Crowding distance in the Pareto frontier.

two adjacent particles in the Pareto frontier, namely particles $i-1$ and $i+1$, is defined as its crowding distance as follows:

$$d_i = \frac{d_{i,1} + d_{i,2}}{2} \tag{48}$$

By measuring the crowding distance formed by the neighboring particles, the density of the particle distribution is obtained. A higher crowding distance indicates a lower density of the particle distribution and higher diversity of the solution. Conversely, a lower crowding distance denotes higher density of the particle distribution and a lower diversity of the solution. To promote the diversity of the solutions, a solution with a higher diversity will be selected in the archive with a stronger possibility. The structure of MOPSOCD applied in the study is illustrated in Fig. 10.

Three thermodynamic parameters, the mass of working fluid, regenerative duration and volume compression ratio, are chosen as the decision variables and their limits are set as

$$5\ \mathrm{g} \le m \le 8\ \mathrm{g}, \tag{49}$$

$$0.001\ \mathrm{s} \le t_r \le 0.003\ \mathrm{s}, \tag{50}$$

$$1.5 \le \lambda \le 5. \tag{51}$$

The output power and the thermal efficiency denoted by Eqs. (45) and (43) are chosen as the two optimization objectives. The population size is set as 200 and maximum generation 2000. The Pareto frontier obtained by the multi-objective optimization is plotted in Fig. 11. With respect to the parameters given above, the ideal point should be located at the top-right, leading to the maximum thermal efficiency and the highest output power. In contrast, the non-ideal point should be located at the bottom-left, leading to the lowest thermal efficiency and the least output power. In Fig. 11, we can observe the conflicting relationship is evident between the thermal efficiency and the output power. It is observed that the optimal solutions are located in $11.31\ \mathrm{kW} \le P \le 61.02\ \mathrm{kW}$ and $9.22\% \le \eta \le 37.27\%$. The blue circle represents the Pareto optimal solution, composing the Pareto frontier. The red star represents the final optimal solution selected by the decision-making method TOPSIS. The corresponding objectives as output power and thermal efficiency are 51.03 kW and 17.50%, and variables as the mass of working fluid, regenerative duration and volume compression ratio are 5.29 g, 0.0017 s and 1.50.

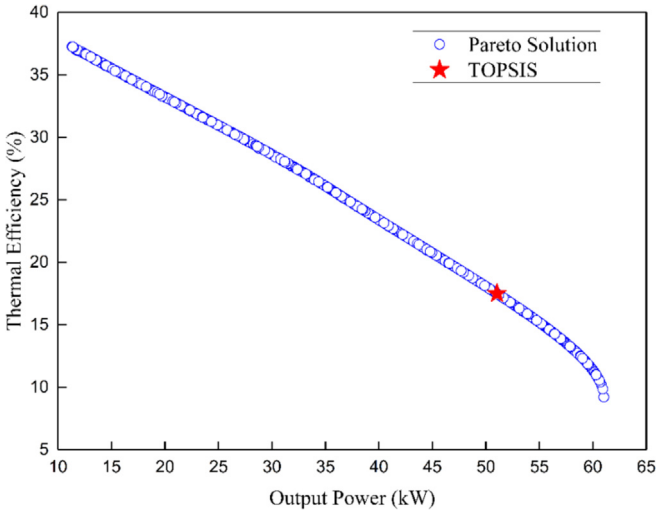

Fig. 11. Pareto optimal frontier in objective space.

The results obtained by multi-objective and single-objective optimizations are compared in Fig. 12. Compared with the optimal result obtained by the single-objective optimization of power, the optimal result through the multi-objective optimization algorithm MOPSOCD and selected by TOPSIS was obtained as 16.37% lower in terms of power, but 89.80% higher in terms of efficiency. Compared with the optimal result obtained by the single-objective optimization of efficiency, the optimal result through the multi-objective optimization algorithm MOPSOCD and selected by TOPSIS was obtained as 53.05% lower in terms of efficiency, but nearly 3.51 times higher in terms of power. In a word, compared with the traditional single-objective optimization, the MOPSOCD algorithm is an effective method for promoting one objective without decreasing the other objective significantly. Therefore, the MOPSOCD algorithm can optimize multiple objectives simultaneously and shows a superiority in balancing different objectives.

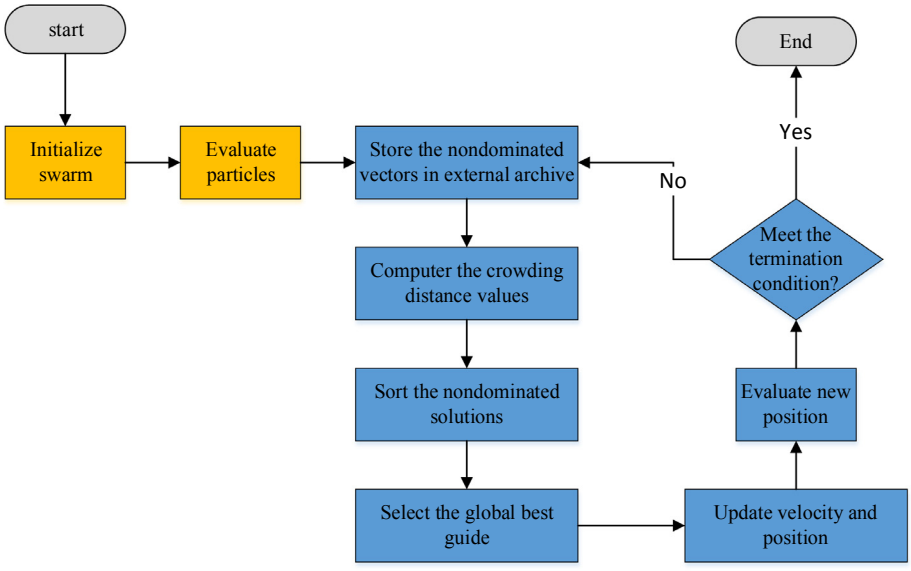

Fig. 10. The flow chart of MOPSOCD.

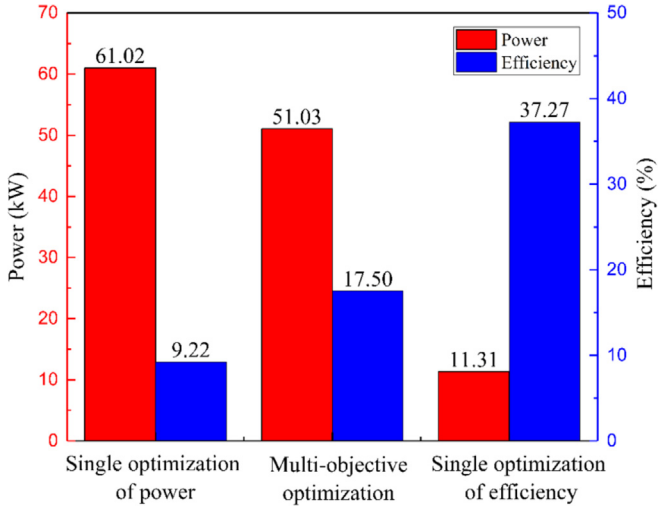

Fig. 12. Comparison of efficiency and power under different optimization methods.

The parameters optimized by the MOPSOCD algorithm has more practical guidance in Stirling engine design and optimization.

3. Conclusion

In this study, we present an irreversible Stirling engine cycle model by taking the heat transfer between the working fluid and external heat reservoirs, irreversible heat transfer during regenerative processes, and polytropic processes in expansion and compression processes into consideration. Polytropic exponents in expansion and compression processes are obtained by the method of thermodynamics for the first time. As a result, we obtain a cycle model that is different from the canonical Stirling cycle but much closer to the real engine, providing a more practical guidance on designing Stirling engines. With given parameters, the thermal efficiency and output power are obtained and compared with the corresponding ideal Stirling cycle. It is observed that the thermal efficiency and output power of the real Stirling engine cycle are obviously lower than those of the ideal Stirling cycle.

To further investigate the performance of the Stirling engine cycle model, the effect of the mass of working fluid, thermal conductance in the expansion stroke, thermal conductance in the expansion stroke, regenerative duration, and volume compression ratio on output power and thermal efficiency are investigated. Among these parameters, the mass of the working fluid, regenerative time, and volume compression ratio are three variables need to be made decision-making with respect to output power and thermal efficiency. Furthermore, thermal efficiency and output power of the proposed model were simultaneously optimized for maximization by the algorithm MOPSOCD. TOPSIS is adopted in decision-making and the result obtained is compared with those obtained by single-objective optimization method. The findings indicate that the optimal result obtained by MOPSOCD exhibits a more desirable performance.

Acknowledgmentsss

This work was supported by the National Natural Science Foundation of China (Grant No. 51736004).

Nomenclature

A	heat transfer area, m^2
c_v	constant volume specific heat capacity, J/(g·K)
C	constant in polytropic process
e	effectiveness
h	convective heat transfer coefficient, W/(m^2·K)
m	mass of working fluid, g
n	number of sub-regenerators
n_H	polytropic index of heating process
n_C	polytropic index of cooling process
P	output power, W
Q	heat, J
R_g	molar-weight-specific gas constant of Helium
S	entropy, J/K
t	time, s
T	temperature, K
U	internal energy, J
V	volume, m^3
W	cycle work, J

Greek symbols

α_h	thermal conductance during heating process, W/K
α_l	thermal conductance during cooling process, W/K
α_r	h_rA_r, W/K
η	efficiency
λ	volume ratio
Σ	relaxation time c_f/α_r, s
τ	duration, s
γ	temperature ratio T_2/T_4

Subscripts

C, c	compression process
e	expansion process
f	working fluid
H, h	high temperature
l	low temperature
r	regeneration
i	ith sub-regenerator

References

[1] Ahmadi MH, Ahmadi MA, Pourfayaz F. Thermal models for analysis of performance of Stirling engine: a review. Renew Sustain Energy Rev 2017;68:168–84.
[2] Ding G, Chen W, Zheng T, Li Y, Ji Y. Volume ratio optimization of Stirling engine by using an enhanced model. Appl Therm Eng 2018;140:615–21.
[3] Xiao G, Huang Y, Wang S, Peng H, Ni M, Gan Z, et al. An approach to combine the Second-order and third-order analysis methods for optimization of a Stirling engine. Energy Convers Manag 2018;165:447–58.
[4] Curzon FL, Ahlborn B. Efficiency of a Carnot engine at maximum power output. Am J Phys 1975;43(1):22–4.
[5] Wu F, Chen LG, Sun FR, Wu C. Finite-time exergoeconomic performance bound for a quantum Stirling engine. Int J Eng Sci 2000;38(2):239–47.
[6] Cheng CH, Yu YJ. Numerical model for predicting thermodynamic cycle and thermal efficiency of a beta-type Stirling engine with rhombic-drive mechanism. Renew Energy 2010;35(11):2590–601.
[7] Blank DA, Davis GW, Wu C. Power optimization of an endoreversible Stirling cycle with regeneration. Energy 1994;19(1):125–33.
[8] Ladas HG, Ibrahim OM. Finite-time view of the Stirling engine. Energy 1994;19(8):837–43.
[9] Dai D, Yuan F, Long R, Liu Z, Liu W. Performance analysis and multi-objective optimization of a Stirling engine based on mopsocd. Int J Therm Sci 2018;124:399–406.
[10] Tlili I. Finite time thermodynamic evaluation of endoreversible Stirling heat engine at maximum power conditions. Renew Sustain Energy Rev 2012;16(4):2234–41.
[11] Kaushik SC, Kumar S. Finite time thermodynamic evaluation of irreversible ericsson and Stirling heat engines. Energy Convers Manag 2001;42(3):295–312.
[12] Kaushik SC, Kumar S. Finite time thermodynamic analysis of endoreversible Stirling heat engine with regenerative losses. Energy 2000;25(10):989–1003.
[13] Wu F, Chen LG, Wu C, Sun FG. Optimum performance of irreversible Stirling engine with imperfect regeneration. Energy Convers Manag 1998;39(8):727–32.
[14] Chen JC, Yan ZJ, Chen LX, Andresen B. Efficiency bound of a solar-driven

Stirling heat engine system. Int J Energy Res 1998;22(9):805–12.
[15] Chen J. The effect of regenerative losses on the efficiency of a Stirling heat engine at maximum power output. Int J Ambient Energy 1997;18(2):107–12.
[16] Wu F, Chen L, Wu C, Sun FR, Zhu YH. Optimization of irreversible magnetic Stirling cryocoolers. Int J Eng Sci 2001;39(4):361–8.
[17] Wu F, Wu C, Chen LG, Sun FR. Performance characteristics of a magnetic Stirling cooler. Int J Energy Res 2002;26(3):217–28.
[18] Ding ZM, Chen LG, Sun ER. Performance optimization of a linear phenomenological law system Stirling engine. J Energy Inst 2015;88(1):36–42.
[19] Tyagi SK, Chen JC, Kaushik SC. Thermoeconomic optimization and parametric study of an irreversible Stirling heat pump cycle. Int J Therm Sci 2004;43(1):105–12.
[20] Chen JC. Minimum power input of irreversible Stirling refrigerator for given cooling rate. Energy Convers Manag 1998;39(12):1255–63.
[21] Tyagi SK, Lin G, Kaushik SC, Chen J. Thermoeconomic optimization of an irreversible Stirling cryogenic refrigerator cycle. International Journal Of Refrigeration-Revue Internationale Du Froid. 2004;27(8):924–31.
[22] Dai DD, Yuan F, Long R, Liu ZC, Liu W. Imperfect regeneration analysis of Stirling engine caused by temperature differences in regenerator. Energy Convers Manag 2018;158:60–9.
[23] Liu W, Liu P, Wang JB, Zheng NB, Liu ZC. Exergy destruction minimization: a principle to convective heat transfer enhancement. Int J Heat Mass Transf 2018;122:11–21.
[24] Liu W, Liu P, Dong ZM, Yang K, Liu ZC. A study on the multi-field Synergy principle of convective heat and mass transfer enhancement. Int J Heat Mass Transf 2019;134:722–34.
[25] Erbay LB, Yavuz H. Analysis of the Stirling heat engine at maximum power conditions. Energy 1997;22(7):645–50.
[26] Ahmadi MH, Ahmadi MA. Thermodynamic analysis and optimization of an irreversible ericsson cryogenic refrigerator cycle. Energy Convers Manag 2015;89:147–55.
[27] Ahmadi MH, Ahmadi MA. Thermodynamic analysis and optimisation of an irreversible radiative-type heat engine by using non-dominated Sorting genetic algorithm. Int J Ambient Energy 2016;37(4):403–8.
[28] Ahmadi MH, Ahmadi MA, Feidt M. Performance optimization of a solar-driven multi-step irreversible brayton cycle based on a multi-objective genetic algorithm. Oil Gas Sci Technol 2016;71(1):16.
[29] Kahraman HT. Metaheuristic linear modeling technique for estimating the excitation current of a Synchronous motor. Turk J Electr Eng Comput Sci 2014;22(6):1637–52.
[30] Kahraman HT, Bayindir R, Sagiroglu S. A new approach to predict the excitation current and parameter weightings of Synchronous machines based on genetic algorithm-based K-nn estimator. Energy Convers Manag 2012;64:129–38.
[31] Ahmadi MH, Ahmadi MA, Mehrpooya M. Investigation of the effect of design parameters on power output and thermal efficiency of a Stirling engine by thermodynamic analysis. Int J Low Carbon Technol 2016;11(2):141–56.
[32] Ahmadi MH, Sayyaadi H, Dehghani S, Hosseinzade H. Designing a solar powered Stirling heat engine based on multiple criteria: maximized thermal efficiency and power. Energy Convers Manag 2013;75:282–91.
[33] Ahmadi MH, Sayyaadi H, Mohammadi AH, Barranco-Jimenez MA. Thermo-economic multi-objective optimization of solar dish-Stirling engine by implementing evolutionary algorithm. Energy Convers Manag 2013;73:370–80.
[34] Duan C, Wang X, Shu S, Jing C, Chang H. Thermodynamic design of Stirling engine using multi-objective particle swarm optimization algorithm. Energy Convers Manag 2014;84:88–96.
[35] Luo ZY, Sultan U, Ni MJ, Peng H, Shi BW, Xiao G. Multi-objective optimization for Gpu3 Stirling engine by combining multi-objective algorithms. Renew Energy 2016;94:114–25.
[36] Raquel CR, Naval PC. An effective use of crowding distance in multiobjective particle swarm optimization. In: Gecco 2005: genetic and evolutionary computation conference, 1 And 2; 2005. p. 257–64.